Intercomparison of Seven Collocated Ground-based Infrared Spectrometer Radiance Observations and Retrieved Thermodynamic Profiles

David D. Turner[1], Bianca Adler[2,3], Laura Bianco[2,3], James M. Wilczak[2*], Vincent Michaud-Belleau[4], and Luc Rochette[5]

[1]NOAA / Global Systems Laboratory, Boulder, CO, USA
[2]Physical Sciences Laboratory, Boulder, CO, USA
[3]Cooperative Institute for Research in the Environmental Sciences, University of Colorado, Boulder, CO, USA
[4]Waxwing Instruments Inc., Quebec City, Quebec, Canada
[5]Telops, Quebec City, Quebec, Canada
[*]Retired

Target journal: Atmospheric Measurement Techniques (AMT)

Correspondence to: David D. Turner (dave.turner@noaa.gov)

Abstract

Thermodynamic profiles, especially in the atmospheric boundary layer (ABL), are essential for many research and operational applications. Ground-based infrared spectrometers (IRS) are commercially available, and thermodynamic profiles in the ABL can be retrieved from these observations at 5-minute resolution or better. This study deployed seven IRS systems within 5 m of each other in Boulder, Colorado, USA, in September-October 2023, providing an opportunity to evaluate the relative accuracy of the measured radiances from these systems as well as the retrieved thermodynamic profiles. The analysis demonstrates that the observed radiances from the seven instruments agree within 1% of the ambient radiance in both opaque and more transparent channels. The differences in the spectral calibration between the instruments were smaller than 0.11 cm^{-1}, relative to the nominal effective wavenumber of the metrology laser of 15799 cm^{-1} (i.e., better than 7.1 ppm). Further, the retrieved temperature and humidity profiles agree with each other well within the uncertainty of the retrieved profiles, and quantities derived from these thermodynamic profiles such as precipitable water vapor and height of the convective boundary layer also agree within their uncertainties. These results demonstrate a high degree of repeatability and precision, and that if these instruments were deployed as part of a network, any differences larger

than the retrieval uncertainty would be associated with real environmental differences and not an artifact of the instrument calibration or retrieval.

1 Introduction

The operational benefits of a network of ground-based dynamic and thermodynamic profilers are becoming more recognized. In 2009, the United States National Research Council wrote of the need to expand ground-based profiling networks to support meteorological and climatological purposes (National Research Council 2009). In the 2010s, the European Union undertook the TOPROF (Towards operational ground-based profiling with ceilometers, Doppler lidars, and microwave radiometers for improving weather forecasts) action to unite national-scale networks into a continent-wide observing facility (Illingworth et al. 2019). More recently, New York State deployed 17 profiling sites as part of its mesonet in 2016; each site hosts Doppler lidars and microwave radiometer profilers. An implicit assumption present in the deployment and utilization of these networks is that identical models of the same instrument are interchangeable: that is, two profiling instruments located immediately adjacent to each other would produce identical observations within their observational uncertainties and that these uncertainties are well-understood and useful for a mesoscale analysis. Without validation of that assumption, one cannot be certain that any difference between two profiler observations made in separate locations is atmospheric in nature. After all, some of the observed differences could be due to differences in the observing system and not differences in the environment. For in situ sensors, laboratory calibrations make it relatively easy to validate their performance in a variety of conditions and affirm their interchangeability in a short period of time. Remote sensing profilers, however, tend to require longer term deployments outdoors in order to assess their performance. Due to the relative paucity of ground-based profilers, it is rare that multiple models of the same instrument sense the same environment simultaneously, and thus the interchangeability assumption remains untested for many profiling systems.

One candidate for a large-scale network deployment is the ground-based infrared spectrometer (IRS). There are two commercially-available IRS systems available today: the Atmospheric Emitted Radiance Interferometer (AERI, Knuteson et al. 2004) and the Atmospheric Sounder Spectrometer by Infrared Spectral Technology (ASSIST, Michaud-Belleau et al. 2025). Both of these ground-based Fourier-transform spectrometers measure downwelling infrared spectra between roughly 3 to 19 μm with a spectral resolution of better than 1 cm^{-1}. Each IRS observation is calibrated against two on-board blackbodies to yield an accurate estimate of the downwelling spectral radiance in the instrument's narrow field of view (which is less than 3 degrees for both IRS systems). This calibration approach provides traceable accuracy over multiple years, which

enables long term trend detection and analysis (Gero and Turner 2011). A weather-hardened enclosure and an automated precipitation-sensing hatch that protects the optics during rain and snow events means that the ASSIST and AERI can be safely deployed in almost any environment. These instruments have found long term success in environments as diverse as ice sheets (Shupe et al. 2013), extreme altitudes (Turner and Mlawer 2010) and complex terrain environments (Adler et al. 2023), midlatitudes (e.g., Degelia et al. 2020), tropical environments (Mlawer et al. 2024), marine environments (Adler et al. 2026), and aboard transoceanic ships (Minnett et al. 2001). As these instruments in their enclosure occupy less than 1 m^3 in volume, they can easily be mounted aboard a variety of platforms, including mobile trailer-based facilities (Wagner et al. 2019).

Since the downwelling spectral radiance observed by IRS is a function of the thermodynamic structure of the atmosphere, it is possible to invert the IRS spectral observations to obtain profiles of temperature and water vapor through a physical or statistical retrieval. Currently, the most prevalent retrieval algorithm is the Tropospheric Remotely Observed Profiling via Optimal Estimation (*TROPoe*) retrieval (Turner and Löhnert 2014, Turner and Blumberg 2019). *TROPoe* uses the line-by-line radiative transfer model LBLRTM (Clough et al. 2005) as the forward model in a Gauss-Newton optimal estimation inversion (Rodgers 2000). This method is a Bayesian framework that iteratively adjusts a first guess of the profile until the modelled spectrum converges to the observed one. *TROPoe* also propagates the various uncertainties (such as measurement and prior uncertainty) through the retrieval so that the retrieved profile is accompanied by total 1-σ uncertainties at each level, which quantifies the measurement error and helps to easily facilitate the assimilation of these observed profiles into numerical weather prediction forecast models (e.g., Hu et al. 2019).

One of the newer applications that requires that there are negligible systematic biases among a group of these remote sensors is when they are deployed in a network to measure advection. Recent work by Wagner et al. (2022) has demonstrated that profiles of water vapor and temperature advection can be derived using a line integral approach around a non-linear arrangement of 3 or more ground-based profilers. However, if there are inconsistencies among the instruments that are not meteorologically driven, then errors in the derived moisture and temperature advection would arise. Similarly, there have been a number of data assimilation experiments using profiles derived from ground-based remote sensors (e.g., Degelia et al. 2020; Chipilski et al. 2022), and non-meteorological differences in the observed profiles would create artifacts into the analysis of the numerical weather prediction model.

NOAA's Physical Sciences Laboratory recently purchased 8 ASSISTs to support fire-weather and other research studies. Two were purchased in 2020 (units 07 and 08), with the other six acquired in 2023 (units 16 – 21). As part of an instrument characterization effort, seven of these systems (unit 07 and units 16 – 21) were deployed on the roof of the David Skaggs Research Center in Boulder, Colorado (39.993 N, -105.262 E, 1670 m

above mean sea level) for approximately one month from mid-September to mid-October 2023. This paper will evaluate the accuracy of the radiance observations relative to each other (section 2) and the relative accuracy of the retrieved thermodynamic profiles (in clear sky and below cloud layers) and other geophysical variables (section 3), with conclusions in section 4.

2. Instrument description

The ASSIST is a ground-based Fourier-transform spectrometer that is designed to operate autonomously. A full description of the ASSIST instrument and its data processing is provided by Michaud-Belleau et al. (2025, henceforth MB25), and this section provides an abbreviated overview of the instrument. The ASSIST measures the downwelling infrared radiance at better than 1 cm^{-1} resolution from 3.0 μm (3300 cm^{-1}) to 19.0 μm (525 cm^{-1}) using two detectors that have sensitivity to radiation in two sub-bands: between 4.9 – 20.0 μm using a mercury cadmium telluride photo conductor (MCT) and between 1.8 to 5.9 μm using an indium antimonide photodiode (InSb). A Stirling cooler is used to keep the detectors at approximately 75 K, which is critical to achieve good signal-to-noise in the observed radiance. A rotating, gold-plated scene mirror is used to routinely view the downwelling radiance from the sky, and that emitted by the two blackbodies. The instrument periodically views two calibration blackbody targets, which have been designed to have high emissivity (> 99.8%) and precision thermistors are used to measure the temperature in multiple locations on this blackbody to better than 5 mK. One of the blackbodies is allowed to float at the ambient temperature, whereas the second blackbody is actively heated and controlled to maintain a temperature of 60°C. The ASSISTs were configured to collect a spectrum every 13 s. As indicated in MB25, each ASSIST typically collects 6 sky samples and then views the ambient and hot blackbodies, after which the pattern is repeated. This results in approximately 3900 sky samples being collected per day. An example of an observed clear sky spectrum is shown in blue in Fig. 1, with the noise level of the observed radiance (multiplied by a factor of 10) shown in red. The spectral bands that *TROPoe* uses to retrieve water vapor and temperature profiles, as well as cloud information, are shown in the figure too, with the primary sensitivity of each band indicated with a W, T, and C, respectively. More information on the retrieval algorithm will be given in section 5.

An enclosure around the instrument protects the interferometer and keeps it, the aft optics, and electronics at laboratory temperatures (i.e., approximately 25°C), and an aluminium hatch is used to protect the fore optics and gold scene mirror from falling precipitation. The design of the enclosure was different for the ASSIST-07, which is on the right-most side of Fig. 2, than that used in the later versions of the ASSIST (numbers 16-21, also

seen in Fig. 2). The random noise level of the observed radiance can be directly computed from the observations following the technique of Revercomb et al. (1988).

The ASSIST calibration uses linear interpolation / extrapolation from two known points: the observed signals and known radiances of the two blackbodies. The radiance from each blackbody is computed from the modelled blackbody emissivity and the temperature observations made by the thermistors embedded within the blackbody itself. As the radiance of the sky is lower than that of the two blackbodies, we are usually extrapolating the radiance from the blackbody observations to the radiance of the sky from its observation. However, while the response of the InSb detector is inherently linear, that of the MCT detector is not and thus a non-linearity correction must be determined beforehand for that detector. This correction coefficient, which is described in detail by MB25, is determined in the factory laboratory as part of the checkout process conducted before the instrument is shipped to a customer. Any errors in this non-linearity correction, as well as those associated with the accuracy of the thermistors in the blackbodies, will be most apparent when the effective sky temperature is far from that of the blackbodies, as that would require the maximum extrapolation of the calibration, and thus would be expected to be most apparent in clear sky scenes at wavenumbers where the atmosphere is most transparent (Fig 3). The radiometric calibration target goal is that the observed downwelling sky radiance is within 1% of the ambient radiation (Knuteson et al. 2004), where the ambient radiance is estimated as a blackbody emission at the air temperature directly at the instrument's sky port.

In addition to radiometric calibration, Fourier-transform spectrometers also need to be spectrally calibrated, so that the spectral features associated with trace gases in the atmosphere are in the right location spectrally. This requires corrections applied to account for both the instrument's finite field-of-view, which allows light from angles other than parallel to the optical axis to enter the instrument and be modulated by the interferometer thereby creating a self-apodizing effect, and to account for any misalignment of the metrology laser that is used to trigger the detector as part of the sampling strategy (MB25). The former is corrected by using laboratory observations (this is also known as the lineshape correction), whereas the second is also determined in the laboratory but can also be easily evaluated in the field by the user. The on-board software corrects for both of these effects, and resamples the observed sky radiance to a specified spectral grid associated with an assumed metrology laser wavenumber of 17599.0 cm^{-1}. Again, full details of these corrections are specified in MB25.

3. General weather conditions

The seven ASSIST units were deployed side-by-side on the top of the NOAA David Skaggs Research Center in Boulder, CO, during this comparison (Fig. 2). The weather conditions during the intercomparison period

were generally warm and dry, and reasonably representative of normal weather conditions for the region. A relatively heavy precipitation event occurred on 14 September 2023; thus, the period for analysis was selected to be 17 September to 11 October. The near-surface air temperatures ranged from a minimum value of 4°C to a maximum value of 29°C, and the near-surface water vapor mixing ratios ranged from 1.5 to 8.4 g kg^{-1}. The precipitable water vapor during this period ranged from 0.3 cm to nearly 1.9 cm. The sky was generally cloud-free for a large fraction of the period.

4. Calibration results

Our first objective was to evaluate the radiometric and spectral calibration of the ASSISTs relative to each other. Because clouds are very efficient emitters of infrared radiance where even small amounts of liquid have a significant downwelling infrared radiance signal (e.g., Turner 2007), we selected clear sky periods during the campaign to evaluate the downwelling radiance observed by the 7 systems. Clear sky scenes are also associated with the lowest downwelling radiance within the infrared atmospheric window, and thus provide a stringent test for the calibration (e.g., see Fig. 3). We identified clear sky periods by identifying periods where the radiance in a transparent atmospheric window channel, such as 900 cm^{-1}, was relatively low (i.e., less than 25 radiance units (RU), where a radiance unit is 1 mW $(m^2\ sr\ cm^{-1})^{-1}$) and the standard deviation over a 5-minute window was less than 2 RU. For this analysis, we required that each clear sky period be at least 60 minutes long to be kept in the analysis. This resulted in over 46,000 clear sky spectra being identified as clear sky.

We first compared the observed radiance in spectral regions that are opaque, such as at 675 cm^{-1} shown in Fig. 4, using a single instrument as the standard. We chose ASSIST-18, to be consistent with MB25 that compared the ASSIST to a collocated AERI during the same period. (The AERI was only available for a couple days during the intercomparison period, as it was transiting from one deployment to another; the comparison of ASSIST-18 with the AERI was presented in MB25.) The dashed lines in Fig. 4 denote the desired radiometric calibration uncertainty of 1% of the ambient radiance (Knuteson et al. 2004), which is the overall radiometric goal of both the AERI and ASSIST. All of the observed points, with a few exceptions, lie well within this desired uncertainty range.

Next, we evaluated the observed radiance in a spectral region that was much more transparent, namely at 985 cm^{-1} (Fig. 5). In this spectral region, the observed radiance is very small due to both clear sky conditions and the relatively low amount of precipitable water vapor over the site during the comparison period. Like the opaque channel, all of the points in the scatterplot between any other ASSIST and ASSIST-18 are well within the 1% ambient radiance bounds for all of the clear sky points.

We evaluated the mean spectral difference in clear sky scenes between ASSIST-18 and the other ASSISTs (Fig. 6). The 1% ambient radiance threshold target is indicated by the spectrally smooth lower and upper bounds in the figure. There is some "spikiness" in the difference plot associated with some slight differences among the instruments associated with the sides of absorption lines and slightly different residual instrument response functions, but generally these are within the 1% ambient radiance and certainly within 2% of the ambient radiance. Like Fig. 1, the spectral regions used for the thermodynamic and cloud retrievals are indicated, and some differences that are appreciably different from zero can be seen there. We will evaluate the impact of these differences in the retrieved profiles in the next section. We can also see that there are several instruments that do not perfectly agree with ASSIST-18 in the infrared window (i.e., between 800 to 1200 cm^{-1}) where the spectral difference is relatively broad; this is due to either slight uncertainties in the non-linearity correction factor or in the blackbody calibration factors (e.g., Table 1), as these uncertainties will translate into their maximum impact where the calibration extrapolation is at its maximum (see Fig. 3). The differences in the atmospheric window may impact the retrieved liquid water path somewhat, and will be investigated in the next section also.

To evaluate the spectral calibration, we utilized the approach outlined in Knuteson et al. (2004). The infrared radiance spectrum observed by the ASSIST-18 was used as the reference, and coincident clear sky spectra from that instrument and each of the others was first interpolated to a very fine spectral resolution by zero-padding the interferogram, and then the spectrum of the other instrument was stretched by a multiplicative factor (f) to find the best agreement in terms of minimum root-mean-square difference (RMSD) with the ASSIST-18 in the 730-740 cm^{-1} region where there are a series of regularly spaced CO_2 absorption lines. The multiplicative factor that gave the lowest RMSD was then used to compute the new effective metrology laser wavenumber; i.e., $\nu_{laser\_eff} = \nu_{laser} * f$, where $\nu_{laser} = 15799.0$ cm^{-1}. Histograms of the differences in $\nu_{laser\_eff} - \nu_{laser}$ are shown in Fig. 7. The instrument with the worst spectral calibration agreement was the ASSIST-16, which had a difference in the effective laser wavenumber of 0.11 cm^{-1} (which translates into 7.1 ppm) (Table 2). The standard deviation in the effective laser wavenumber differences was between 0.9 and 2.6 ppm, which is very similar to the results shown for two AERIs in Knuteson et al (2004). Are the sizes of these spectral calibration differences important for the retrieved thermodynamic profiles? This question will be evaluated in section 5.

5. Profile results

5.1 Retrieval background

One of the primary applications for ground-based infrared spectrometers is to measure profiles of temperature and water vapor in the atmospheric boundary layer above the instrument. However, these profiles

need to be retrieved from the observed radiance, as mathematically it is an ill-posed problem, and thus the retrieval method matters (e.g., Maahn et al. 2020). The original retrieval developed for the AERI was constructed in the mid-1990s (Smith et al. 1999; Feltz et al. 1998); however, that particular algorithm had a number of limitations that was ultimately addressed by the *AERIoe* algorithm (Turner and Löhnert 2014). *AERIoe* has subsequently evolved, and is now called *TROPoe* because of its flexibility to retrieve thermodynamic profiles and cloud information not only from ground-based IRS instruments, but also microwave radiometers, lidars, and other instruments (e.g., Turner and Blumberg 1999; Turner and Löhnert 2021, Bianco et al. 2024).

TROPoe is a physical-iterative retrieval that is based upon optimal estimation (Rodgers 2000). Starting from a first-guess profile, it computes a simulated observation from a forward model that is compared against the true observation, and if there are significant differences above the instrument's noise level, then the algorithm updates the atmospheric profile using the sensitivity of the forward model (i.e., its Jacobian). The retrieval is constrained by a prior dataset, which provides a mean climatology and importantly the level-to-level uncertainty in the climatology in the form of a covariance matrix. Full details of the *TROPoe* retrieval algorithm, including its convergence criteria and how it estimates the uncertainties of each retrieval, are provided in Turner and Löhnert (2014). *TROPoe* version 0.18 was used to retrieve profiles and cloud properties from all of the ASSISTs at 5-minute resolution, which uses the larger of the spectral noise from the instrument or the preset radiometric noise floor suggested by Adler et al. (2024).

For this comparison, we used an a-priori dataset derived from approximately 1,900 radiosondes launched by the National Weather Service in Denver, CO; the launch site is 43 km southeast of the DSRC site in Boulder. The uncertainty of the temperature in this prior is 9.3°C at the surface and decreases to 5.0°C at 4 km; the uncertainties in the water vapor mixing ratio are 2.5 and 1.1 g kg^{-1} at the surface and 4 km, respectively. Thus, with these large uncertainties in the prior, the prior is not over constraining the retrieval.

An example of the retrieved temperature over a 4-day period from 27-30 September is shown in the top panel of Fig. 8. A clear diurnal cycle is seen, with near surface inversions forming during the night, and warmer convective boundary layers forming during the day. The temperature differences between two ASSISTs (units 16 and 21; note that the differences in the spectral calibration relative to ASSIST18 are of the opposite sign in Fig. 7) is shown in the bottom panel, demonstrating that the differences are small with some differences approaching +0.3°C around 1 km and a slight negative difference above 2 km. A comparison of the retrieved water vapor mixing ratio profiles for the same time period is shown in Fig. 9, which also demonstrates both significant variability in the water vapor profile structure and very good agreement (absolute differences generally less than 0.2 g kg^{-1}) between the two ASSIST instruments.

5.2 Clear sky profile results

The mean difference profiles in the retrieved temperature (left) and water vapor mixing ratio (right) profiles from ASSIST-18 and the other ASSISTs are shown in Fig. 10. This analysis included 3,049 matched profiles; i.e., these are times when all 7 instruments provided profiles in clear skies simultaneously. In both panels, the dashed lines indicate the uncertainty bounds ($\pm 1\sigma$) of the retrieval (i.e., the uncertainty computed by *TROPoe*). The absolute values of the mean difference profiles are all much smaller than the uncertainty of the retrieval. Indeed, the absolute values of the mean difference profiles are less than 0.2°C below 2 km for all ASSISTs (relative to ASSIST-18) and only ASSIST-21 differs more than this (up to 0.3°C) at 3 km. The agreement in water vapor is also excellent (Fig 10, right), with all instruments agreeing with ASSIST-18 to better than 0.15 g kg^{-1} below 3 km with the exception of ASSIST-20, which has a larger disagreement of 0.25 g kg^{-1} from the surface to about 800 m. It is interesting to note that the instrument that has the poorest agreement in spectral calibration, ASSIST-16 (Fig. 7), relative to ASSIST-18 is not an outlier in Fig. 10, suggesting that spectral calibration errors within 0.12 cm^{-1} are acceptable for thermodynamic profiling.

Figure 11 looks at the standard deviation profiles associated with the mean difference profiles shown in Fig. 10. The standard deviation between any other ASSIST and ASSIST-18 were essentially identical, further highlighting the consistency of the profiling among any of the ASSIST instruments. Furthermore, these standard deviation profiles are markedly smaller than the *TROPoe* uncertainty profiles illustrated by the dashed lines, except for the lowest 100 m – the uncertainties below 100 m are investigated in detail by Letizia et al. (2025) using a tall tower.

TROPoe derives many other useful geophysical variables from the retrieved profiles (e.g., Blumberg et al. 2017). Figure 12 shows the comparison of the derived precipitable water vapor (PWV) and height of the planetary boundary layer (PBLH) during the coincident clear sky periods. The PWV derived from the ASSIST-18's observations are slightly higher, approximately 0.1 to 0.3 mm; recall that the range of PWV was from 3 to 19 mm during the evaluation period. The PBLH is derived from the retrieved temperature profile using a parcel approach (i.e., to find a height where the potential temperature is larger than the near-surface value), which has been demonstrated to be a good estimate of the PBLH during daytime conditions (Lemone et al. 2013). The mean daytime PBLH during this evaluation period was 1330 m (with a standard deviation of 665 m), and the mean difference in the derived PBLH is less than 125 m for all systems for the 865 coincident points.

5.3 Cloudy sky profile results

Retrievals in cloudy situations from ground-based IRS instruments are more challenging, because the infrared emission from clouds is significantly larger than that from the atmosphere around the clouds. During the

evaluation period, there were relatively few clouds but when they existed, most of the clouds were fair weather cumulus, with a mean liquid water path (LWP) retrieved from the ASSIST of 23 g m^{-2} with a standard deviation of 17 g m^{-2}. *TROPoe* retrieves LWP from the infrared radiance observations also (Turner and Löhnert 2014), and the mean LWP biases between the ASSIST-18 and the other ASSISTs during these cloudy scenes were essentially zero (Fig. 13, top).

Thermodynamic profiles can only be retrieved from ground-based IRS from the surface to cloud base, as even though the overhead clouds were generally not opaque, they still greatly attenuate the radiance emitted by the atmosphere above the clouds. Selecting the cases where the cloud base was between 3 and 4 km, there were 220 cases in our 1-month evaluation period. The comparison of the mean and standard deviation of the differences in the retrieved temperature and humidity profiles in these cloudy cases, relative to ASSIST-18, are almost identical to the clear sky results shown in Figs. 10 and 11 and thus are not shown. As we are interested in how the retrievals between any two ASSISTs compare in clear skies vs cloudy conditions, we wanted to find a more detailed metric.

Thus, we evaluated the retrieved profiles using the modified Taylor plots used in Turner and Löhnert (2014). For each matched profile *i* between ASSIST-18 (*A18*) and the other ASSIST (*Ax*), the correlation between the two matched profiles from the surface to 3 km ($r_{Ax,i}$) and the ratio of the standard deviation of the profile from the surface to 3 km divided by the standard deviation of the profile from the ASSIST-18 ($rsd_{Ax,i}$), are computed as

$$r_{Ax,i} = correlation\left(\phi_{Ax}(i, 0.0 < z < 3.0), \phi_{A18}(i, 0.0 < z < 3.0)\right)$$

$$rsd_{Ax,i} = \frac{sd_{Ax,i}}{sd_{A18,i}}$$

where

$$sd_i = \sqrt{\frac{\sum_{z=0.0}^{z=3.0} \left(\phi(i,z) - \overline{\phi(i)}\right)^2}{n-1}}$$

where ϕ is either temperature (T) or water vapor mixing ratio (q), the overbar denotes the mean value between the surface and 3 km, and *n* is the number of levels in the profile between the surface and 3 km. Ideally, if the profiles matched identically, then both $r_{Ax,I}$ and $rsd_{Ax,I}$ would equal 1; this would denote that the amount of variability in each profile is the same and the variations in the two profiles are well correlated. Figure 14 shows the mean r_{Ax} and rsd_{Ax} values (i.e., computed over all samples *i*) for clear skies (open squares) and cloudy cases where the cloud base heights were between 3 and 4 km (filled circles). Note the excellent mean correlation between any two instruments for both T and q, with *r* values above 0.985. For temperature, the standard deviation

ratio (rsd_{Ax}) is also extremely close to 1. Interestingly, when there are clouds, there is slightly higher correlation in the retrieved temperature profiles; this is because of the increased optical depth at the cloud base height due to the liquid water emission. The standard deviation ratio for water vapor is a bit larger, with values up to 1.2; this demonstrates that the ASSIST-18 has slightly less vertical variability in its retrieved profiles than the other ASSISTs, even though the correlation between the profiles is still very high (> 0.985). Similar to the temperature profile results, the correlation values in the water vapor profile comparisons are slightly higher and the standard deviation ratios are slightly closer to the ideal value of 1 when there are clouds overhead relative to clear sky scenes.

We also evaluated the derived PBLH in daytime cloudy situations. These results, shown in Fig. 13 (bottom panel), demonstrate that the absolute value of the mean bias between any two instruments is less than 150 m. This is almost identical to the mean absolute value of 125 m bias seen in clear skies (Fig. 12 bottom).

6. Conclusions

Thermodynamic profiles, especially in the atmospheric boundary layer (ABL) at high temporal resolution, are essential for many operational and experimental applications. For many of these applications, such as to initialize a mesoscale weather model, networks of instruments capable of providing these profiles are needed. Ground-based infrared spectrometers (IRS) are one technology that has demonstrated good accuracy in thermodynamic profiling of the ABL in both stable and unstable conditions (e.g., Blumberg et al. 2017) and has reasonably high information content in the ABL relative to other technologies (Bianco et al. 2024; Turner and Löhnert 2021; Löhnert et al. 2009).

This study evaluated the relative accuracy between 7 collocated IRS instruments during an approximate 1-month deployment in Boulder, Colorado, USA. We demonstrated that downwelling infrared radiance observed by the seven instruments all agreed well within the 1% ambient radiance specification of the instrument in both opaque and transparent channels. We determined that the spectral calibration differences between instruments was less than 7.1 ppm, and demonstrated that differences of this magnitude were not important for thermodynamic profiling.

Using the *TROPoe* retrieval framework, thermodynamic profiles were retrieved from the 7 instruments. A comparison of clear sky temperature and humidity profiles demonstrated mean biases that were very close to zero, and well within the uncertainty estimate of the retrieval itself. The comparison of profiles below cloud base in cloudy conditions exhibited the same characteristics, namely very small biases near zero that were well within the retrieval uncertainties. An evaluation using the modified Taylor plots demonstrated that both clear and cloudy

results had extremely high correlation coefficients ($r > 0.985$) between two ASSISTs, and standard deviation ratios close to 1 for temperature and less than 1.2 for water vapor. Interestingly, the correlation between any two instruments as seen in the Taylor diagrams was slightly higher in cloudy cases than clear sky cases, suggesting that the increased optical depth at the cloud base height was adding a slight amount of additional information to the retrieval in cloudy cases. Importantly, the slight differences seen in Fig. 6 (i.e., the spikes in the spectral differences) associated with small differences in accounting for the variability in the response function from instrument to instrument, which was discussed in section 4, has no appreciable impact on the retrieved thermodynamic profiles.

This comparison was performed in the autumn at a high elevation site in Boulder, Colorado, and the range of water vapor was relatively dry with the maximum PWV of approximately 1.9 cm. A natural question is: "Would these results be the same if the same comparison was performed in a much more humid environment with larger PWV values?" None of the calibration parameters (i.e., table 1) depend on the actual environment (i.e., they are determined in the laboratory before the instrument is deployed), and thus the question simplifies to how do the uncertainties in these parameters impact the calibrated radiance as the environment changes. This question is addressed using Fig 3: an environment with larger PWV will both be warmer (i.e., the ambient blackbody is warmer) and the amount of extrapolation to get to the scene's radiance will be smaller. Thus, the largest radiometric calibration uncertainty occurs when the day is warm but the PWV is small. Furthermore, the spectral calibration does not depend on the environment at all. Thus, it is expected that the agreement in the thermodynamic profiles would be essentially the same in a warmer, moister environment.

This paper focused only on the evaluation of the calibration of the MCT band (i.e., the 525-1800 cm^{-1} spectral region), and the thermodynamic profiles that were retrieved from spectral subsets of this band. The ASSISTs also measure downwelling radiance in the InSb band, which covers the 1800 to 3300 cm^{-1} spectral region. We wanted to first evaluate the adequacy of the laboratory procedures that determined the calibration parameters for the MCT's nonlinearity correction, finite field-of-view correction, and spectral calibration to ensure that the approach used in the laboratory to determine these parameters was adequate. As very few researchers have used data from the InSb band from either AERIs or ASSISTs (e.g., Turner and Holz 2005; Yurganov et al. 2010), this was a lower priority and the calibration parameters for the InSb band were determined after this intercomparison exercise. However, this study confirmed that the procedures used in the laboratory to derive the needed instrument-specific coefficients are effective, and thus the company has adopted them for both the MCT and InSb bands for all future ASSISTs.

These results demonstrate the robustness of both the ASSIST's calibration and the *TROPoe* retrieval framework for thermodynamic profiling in a network, as any significant/meaningful differences seen between

instruments would be atmospheric in origin and not associated with either the instrument's calibration or the retrieval framework. This provides confidence when analyzing data collected by multiple IRS instruments during campaigns such as the Plains Elevated Convection at Night (PECAN; Geerts et al. 2017), American Wake Experiment (AWAKEN; Moriarty et al. 2025), and the third Wind Forecast Improvement Project (WFIP-3).

Code availability.

The analysis code used in this work was written in IDL, which is available via doi: 10.5281/zenodo.17228423.

Data Availability Statement.

The data used in this research effort are available via zenodo via doi: 10.5281/zenodo.17228423.

Author Contributions.

All of the authors collaborated in the development of this project. VMB and LR ensured that all instruments had the correct laboratory calibration applied, and the detailed day-to-day monitoring of the instruments during the analysis period was done by BA, LB, and VMB. DDT developed the analysis code, and all coauthors evaluated and discussed the results. The manuscript was written by DDT with contributions from all coauthors.

Competing Interests

At least one of the (co-)authors is a member of the editorial board of Atmospheric Measurement Techniques.

Acknowledgments.

This work was supported primarily by the NOAA Atmospheric Science for Renewable Energy Program. This research was additionally supported by NOAA cooperative agreement NA22OAR4320151 for the Cooperative Institute for Earth System Research and Data Science (CIESRDS). The scientific results and conclusions, as well as any views or opinions expressed herein, are those of the authors and do not necessarily reflect those of OAR or the Department of Commerce.

References

Adler, B., Wilczak, J.M., Bianco, L., Baiteau, L., Cox, C.J., de Boer, G., Djalalova, I.V., Gallagher, M.R., Intrieri, J.M., Meyers, T.P., Myers, T.A., Olson, J.B., Pezoa, S., Sedlar, J., Smith, E.N., Turner, D.D., and White, A.B.: Impact of seasonal snow-cover change on the observed and simulated state of the atmospheric boundary layer in a high-altitude mountain valley. *J. Geophys. Res*., **128**, e2023JD038497, doi:10.1029/2023JD038497, 2023.

Adler, B., Turner, D.D., Bianco, L., Djalalova, I.V., Myers, T., and Wilczak, J.M.: Improving solution availability and temporal consistency of an optimal-estimation physical retrieval for ground-based thermodynamic profiling. *Atmos. Meas. Technol*., 17, 6603-6624, doi:10.5194/amt-17-6603-2024, 2024.

Adler, B., Bianco, L., Turner, D.D., Olson, J.B., Sun, X., Gebauer, J., Bodini, N., Letizia, S., and Wilczak, J.M.: Multi-season evaluation of temperature and wind in the marine boundary layer along the United States northeast coast in the High-Resolution Rapid Refresh Model. *Geosci. Model Dev*., doi: 10.5194/egusphere-2026-97, submitted, 2026.

Blumberg, W.G., Wagner, T.J., Turner, D.D., and Correia Jr., J.: Quantifying the accuracy and uncertainty of diurnal thermodynamic profiles and convection indices derived from the Atmospheric Emitted Radiance Interferometer. *J. Appl. Meteor. Clim*., 56, 2747-2766, doi:10.1175/JAMC-D-17-0036.1, 2017.

Bianco, L., Adler, B., Bariteau, L., Djalalova, I.V., Myers, T., Pezoa, S., Turner, D.D., and Wilczak, J.M.: Sensitivity of thermodynamic profiles retrieved from ground-based microwave and infrared observations to additional input data from active remote sensing instruments and numerical weather prediction models. *Atmos. Meas. Technol*., 17, 3933-3948, doi:10.5194/amt-17-3933-2024, 2024

Chipilski, H.G., Wang, X., Parsons, D.B., Johnson, A., and Degelia, S.K.: The value of assimilating different ground-based profiling networks on forecasts of bore-generating nocturnal convection. *Month. Wea. Rev.*, 150, 1273-1292, doi:10.1175/MWR-D-21-0193.1, 2022.

Clough, S.A., Shephard, M.W., Mlawer, E.J., Delamere, J.S., Iacono, M.J., Cady-Pereira, K., Boukabara, S., and Brown, P.D.: Atmospheric radiative transfer modeling: A summary of the AER codes. *J. Quant. Spectroc. Radiative Trans.*, **91**, 233-244, doi:10.1016/j.jqsrt.2004.05.058, 2005.

Degelia, S.K., Wang, X., Stensrud, D.J., and Turner, D.D.: Systematic evaluation of the impact of assimilating a network of ground-based remote sensing profilers for forecasts of nocturnal convection initiation during PECAN. *Month. Wea. Rev.*, 148, 4703-4728, doi:10.1175/MWR-D-20-0118.1, 2020.

Feltz, W.F., Smith, W.L., Knuteson, R.O., Revercomb, H.E., Woolf, H.M., and Howell, H.B.: Meteorological applications of temperature and water vapor retrievals from the ground-based Atmospheric Emitted Radiance Interferometer (AERI). *J. Appl. Meteor.*, **37**, 857-875, 1998.

Geerts, B., and coauthors: The 2015 Plains Elevated Convection At Night field project. *Bull. Amer. Meteor. Soc.*, **98**, 767 – 786, 2017.

Gero, P.J., and Turner, D.D.: Long-term trends in downwelling spectral infrared radiance over the U.S. Southern Great Plains. *J. Climate*., 24, 4831-4843, doi:10.1175/2011JCLI4210.1, 2011.

Hu, J., Yussouf, N., Turner, D.D., Jones, T.A., and Wang, X.: Impact of ground-based remote sensing boundary layer observations on short-term probabilistic forecasts of a tornadic supercell event. *Wea. Forecasting*, **34**, 1453-1476, doi:10.1175/WAF-D-18-0200.1, 2019.

Illingworth, A.J., and coauthors: How can existing ground-based profiling instruments improve European weather forecasts? *Bull. Amer. Meteor. Soc.*, doi:10.1175/BAMS-D-17-0231.1, 2019.

Knuteson, R. O., Revercomb, H.E., Best, F.A., Ciganovich, N.C., Dedecker, R.G., Dirkx, T.P., Ellington, S.C., Feltz, W.F., Garcia, R.K., Howell, H.B., Smith, W.L., Short, J.F., and Tobin, D.C.: Atmospheric Emitted Radiance Interferometer. Part II: Instrument performance. *J. Atmos. Oceanic Technol*., 21, 1777-1789, 2004.

Lemone, M.A., Tewari, M., Chen, F., and Dudhia, J.: Objectively determined fair-weather CBL depths in the ARW-WRF model and their comparison to CASES-97 observations. *Mon. Wea. Rev*., 141, 30-54, doi:10.1175/MWR-D-12-00106.1, 2013.

Letizia, S., Turner, D.D., Abraham, A., Rochette, L., and Moriarty, P.J.: Temperature profiling at the American WAKE Experiment (AWAKEN): Methodology and uncertainty quantification. *Wind Energy Sci*., doi:105194/wes-2025-198, submitted, 2025

Löhnert, U., Turner, D.D., and Crewell, S.: Ground-based temperature and humidity profiling using spectral infrared and microwave observations. Part 1: Simulated retrieval performance in clear sky conditions. *J. Appl. Meteor. Clim.*, **48**, 1017-1032, doi:10.1175/2008JAMC2060.1, 2009.

Maahn, M., Turner, D.D., Löhnert, U., Posselt, D.J., Ebell, K., Mace, G.G., and Comstock, J.M.: Optimal estimation retrievals and their uncertainties: What every atmospheric scientist should know. *Bull. Amer. Meteor. Soc*., 101, E1512-E1523, doi:10.1175/BAMS-D-19-0027.1, 2020.

Michaud-Belleau, V., Gaudreau, M., Lacoursiere, J., Boisvert, E., Ravelomanantsoa, L., Turner, D.D., and Rochette, L.: The Atmospheric Sounder Spectrometer by Infrared Spectral Technology (ASSIST): Instrument design and signal processing. *Atmos. Meas. Tech*., **18**, 3585-3609, doi:10.5194/amt-18-3585-2025, 2025

Minnett, P.J., Knuteson, R.O., Best, F.A., Osborne, B.J., Hanafin, J.A., and Brown, O.B.: The Marine-Atmospheric Emitted Radiance Interferometer: A high-accuracy, seagoing infrared spectroradiometer. *J. Atmos. Oceanic Sci.*, 18, 994-1013, 2001.

Mlawer, E.J., Mascio, J., Turner, D.D., Payne, V.E., Flynn, C.J., and Pincus, R.: A more transparent infrared window. *J. Geophys. Res*., **129**, e2024JD041366, doi:10.1029/2024JD041366, 2024.

Moriarty, P., and 35 coauthors: Wind farm atmosphere interactions as seen in the American WAKE experimeNt (AWAKEN). *Bull. Amer. Meteor. Soc*., submitted, 2025.

National Research Council (NRC) Committee on Developing Mesoscale Meteorological Observational Capabilities to Meet Multiple National Needs: Observing Weather and Climate from the Ground Up: A Nationwide Network of Networks. National Academies Press, 234 pp., 2009.

Revercomb, H.E., Buijs, H., Howell, H.B., LaPorte, D.D., Smith, W.L., and Sromovsky, L.A.: Radiometric calibration of IR Fourier transform spectrometers: Solution to a problem with the high-resolution interferometer sounder. *Appl. Opt.*, 27, 3210-3218, 1988.

Rodgers, C.D.: *Inverse Methods for Atmospheric Sounding: Theory and Practice*. Series on Atmospheric, Oceanic, and Planetary Physics, Vol. 2, World Scientific, 238 pp., 2000.

Shupe, M.D., Turner, D.D., Walden, V.P., Bennartz, R., Cadeddu, M.P., Castellani, B.B., Cox, C.J., Hudak, D.R., Kulie, M.S., Miller, N.B., Neely III, R.R., Neff, W.D., and Rowe, P.M.: High and dry: New observations of tropospheric and cloud properties above the Greenland ice sheet. *Bull. Amer. Meteor. Soc.*, **94**, 169-186, doi:10.1175/BAMS-D-11-00249.1, 2013.

Smith, W.L., Feltz, W.F., Knuteson, R.O., Revercomb, H.E., Woolf, H.M., and Howell, H.B.: The retrieval of planetary boundary layer structure using ground-based infrared spectral radiance measurements. *J. Atmos. Oceanic Technol.*, **16**, 323-333, 1999.

Turner, D.D.: Improved ground-based liquid water path retrievals using a combined infrared and microwave approach. *J. Geophys. Res*., 112, D15204, doi:10.1029/2007JD008530, 2007.

Turner, D.D., and Holz, R.E.: Retrieving cloud fraction in the field-of-view of a high-spectral-resolution infrared radiometer. *IEEE Geosci. Remote Sens. Lett.*, **3**, 287-291, doi:10.1109/LGRS.2005.850533, 2005.

Turner, D.D., and Mlawer, E.J.: The Radiative Heating in Underexplored Bands Campaigns (RHUBC). *Bull. Amer. Meteor. Soc.*, **91**, doi:10.1175/2010BAMS2904.1, 2010.

Turner, D. D., and Löhnert, U.: Information content and uncertainties in thermodynamic profiles and liquid cloud properties retrieved from the ground-based Atmospheric Emitted Radiance Interferometer (AERI). *J. Appl. Meteor. Climatol*., 53, 752-771, doi:10.1175/JAMC-D-13-0126.1, 2014.

Turner, D.D., and Blumberg, W.G.: Improvements to the AERIoe thermodynamic profile retrieval algorithm. *IEEE Selected Topics Appl. Earth Obs. Remote Sens.*, 12, 1339-1354, doi:10.1109/JSTARS.2018.2874968, 2019.

Turner, D.D., and Löhnert, U.: Ground-based temperature and humidity profiling: Combining active and passive remote sensors. *Atmos. Meas. Technol*., 14, 3033-3048, doi:10.5194/amt-14-3033-2021, 2021

Wagner, T.J., Klein, P.M., and Turner, D.D.: A new generation of ground-based mobile platforms for active and passive profiling of the boundary layer. *Bull. Amer. Meteor. Soc.*, 100, 137-153, doi:10.1175/BAMS-D-17-0165.1, 2019.

Wagner, T.J., Turner, D.D., Heus, T., and Blumberg, W.G.: Observing profiles of derived kinematic field quantities using a network of profiling sites. *J. Atmos. Oceanic Tech.*, 39, 335-351, doi:10.1175/JTECH-D-21-0061.1, 2022.

Yurganov, L., McMillan, W., Wilson, C., Fischer, M., Biraud, S., and Sweeney, C.: Carbon monoxide mixing ratios over Oklahoma between 2002 and 2009 retrieved from Atmospheric Emitted Radiance Interferometer spectra. *Atmos. Meas. Techniq.,* **3**, 1319-1331, doi:10.5194/amt-3-1319-2010, 2010

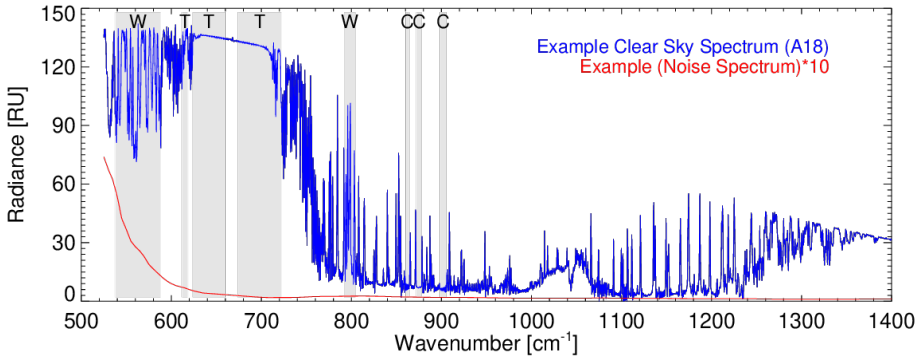

Figure 1: An IR spectrum observed by ASSIST-18 (blue), with its radiometric uncertainty (red), where this uncertainty spectrum has been multiplied by 10 to make it easier to see. Spectral regions used by *TROPoe* are highlighted with the grey background. 1 radiance unit (RU) equals 1 mW $(m^2\ sr\ cm^{-1})^{-1}$. See text for more details.

Figure 2: The 7 ASSISTs on the top of the NOAA building in Boulder, CO. The ASSIST-07 has a slightly different enclosure than the others, and is seen on the righthand side of the image. Photo by Laura Bianco.

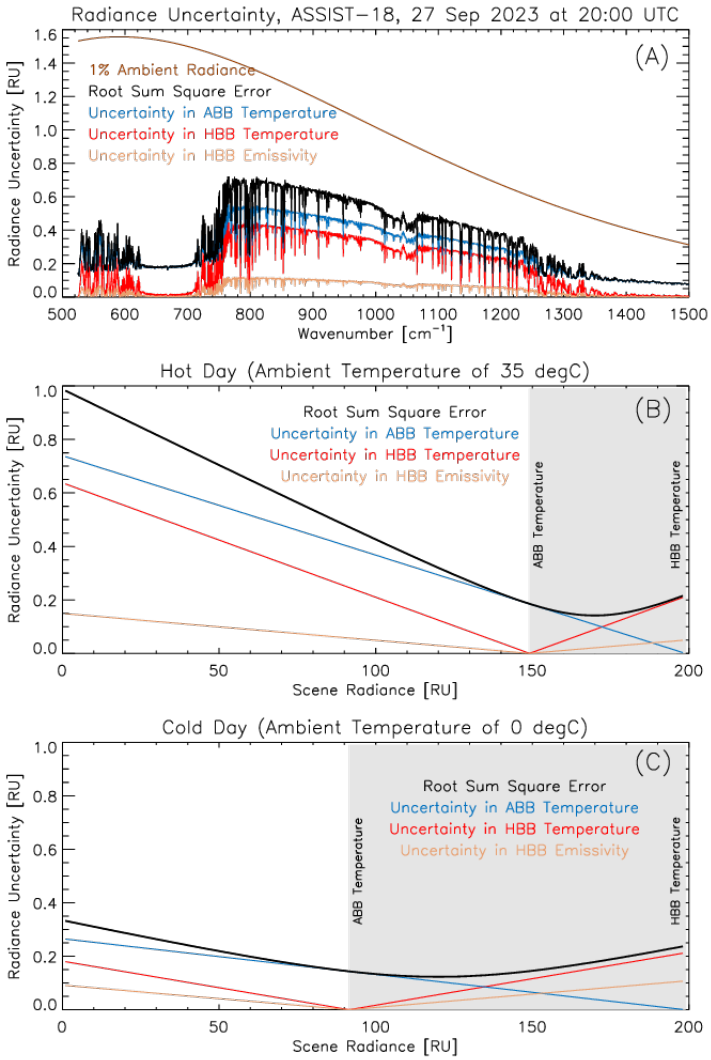

Figure 3: Panel a: The total 3σ radiometric uncertainty (black), which is the root sum of square of the individual contributions associated with the 3σ uncertainties of the temperature of the hot (red) and ambient (blue) blackbodies and the 3σ uncertainty in the emissivity of the hot blackbody (orange). The assumed uncertainties are given in Table 1. The brown line indicates the 1% ambient radiance, demonstrating that total 3σ uncertainty is less than the 1% of the ambient radiance. Panels b and c illustrate how the radiometric uncertainties at 800 cm^{-1} extrapolate to lower scene temperatures for a warm day (ambient temperature of 35°C) and a cold day (ambient temperature of 0°C).

Table 1: Calibration uncertainties assumed for Fig. 3. These are 3σ values.

Parameter	Value Assumed	Uncertainty Estimate (3σ)
Hot Blackbody Temperature	333 K	0.1 K
Ambient Blackbody Temperature	Variable	0.1 K
Hot and Ambient Blackbody Emissivity	0.996	0.001

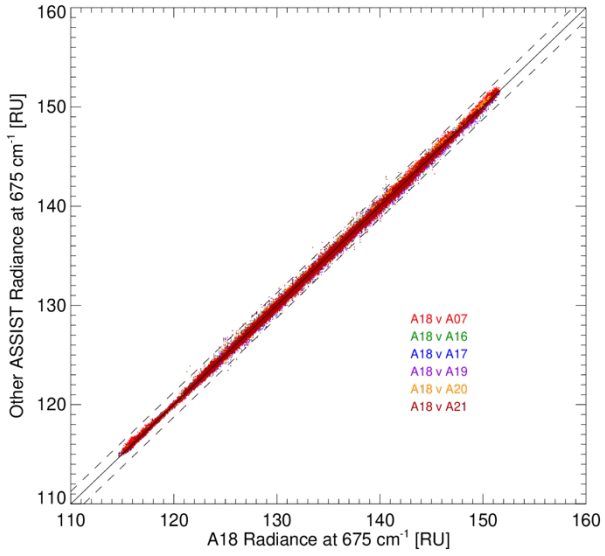

Figure 4: Comparison of the observed radiance from ASSIST-18 at an opaque wavenumber relative to the other ASSISTs during clear sky periods in Sep-Oct 2023.

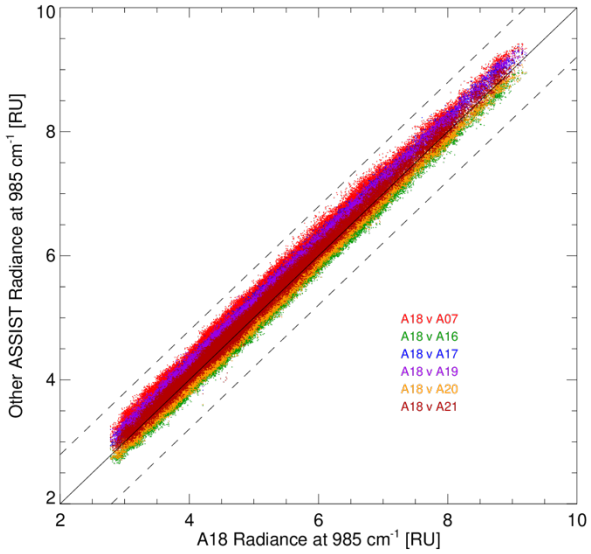

Figure 5: Similar to Fig. 4, but for a semi-transparent wavenumber.

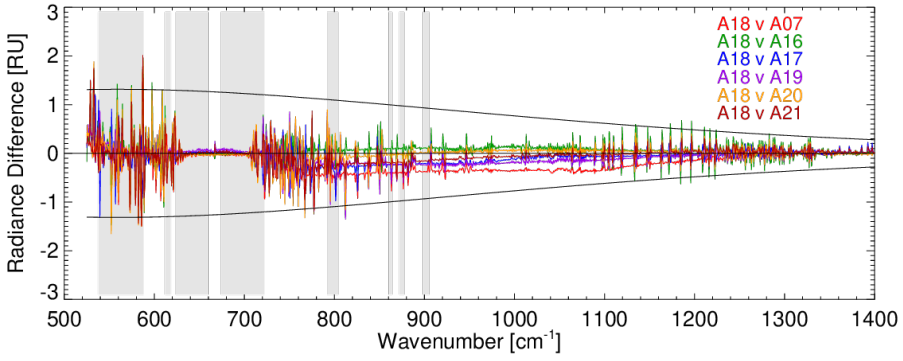

Figure 6: Mean spectral biases of the different ASSISTs relative to ASSIST-18 computed during clear sky periods in the Sep-Oct 2023 period.

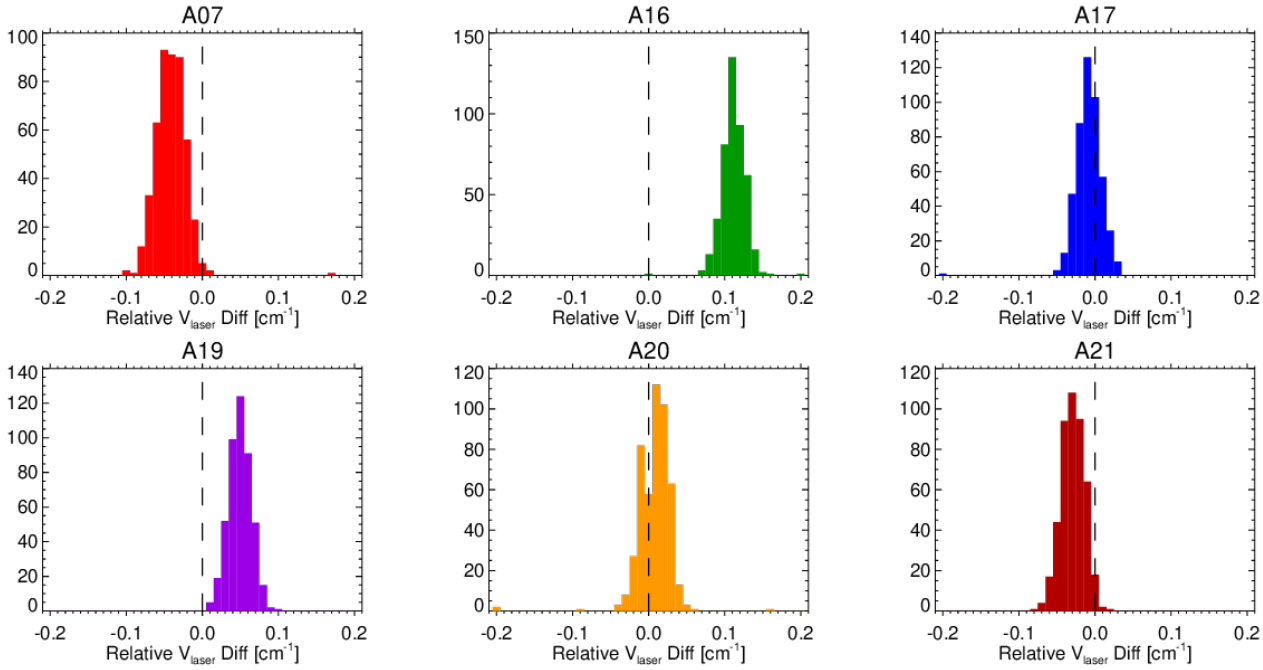

Figure 7: The relative difference in spectral calibration in units of effective laser wavenumber [cm^{-1}], using the A18 instrument as the baseline, for the 12-h clear sky period on 7 Oct 2023. See text for details.

Table 2: Statistics on the relative difference in the spectral calibration relative to ASSIST-18, in units of the effective laser wavenumber [cm^{-1}] and parts per million [ppm].

Instrument	Mean [cm^{-1}]	Mean [ppm]	StdDev [cm^{-1}]	StdDev [ppm]
A07	-0.0414	-2.6	0.0203	1.3
A16	0.1127	7.1	0.0297	1.9
A17	-0.0086	-0.5	0.0240	1.5
A19	0.0494	3.1	0.0150	0.9
A20	0.0061	0.4	0.0418	2.6
A21	-0.0293	-1.9	0.0153	1.0

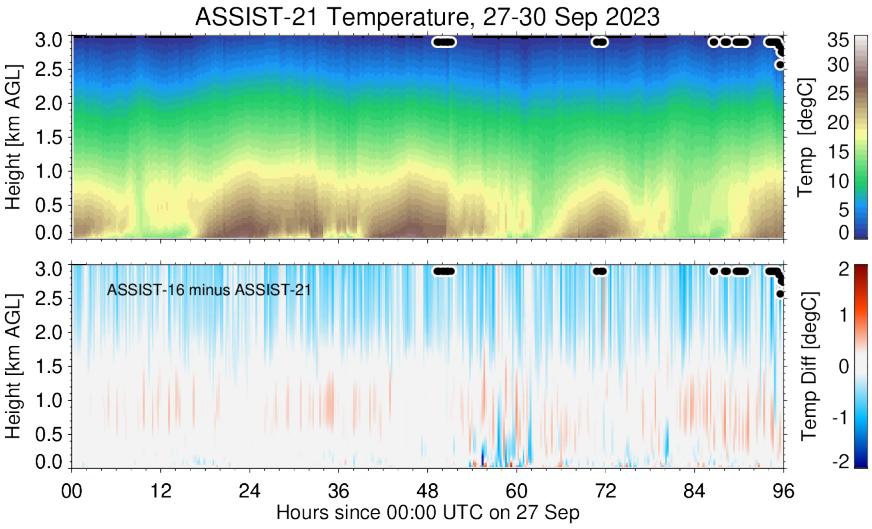

Figure 8: Time-height cross-section of temperature retrieved from ASSIST-21 on 27-30 Sep 2023 in Boulder, CO (top panel), and the difference in the retrieved temperature from ASSIST-16 and ASSIST-21 during the same period (bottom). Filled circles indicate the presence of clouds with liquid water path at or above the height of the symbol (i.e., some clouds existed just above 3 km, and the filled circles denote samples that have clouds overhead).

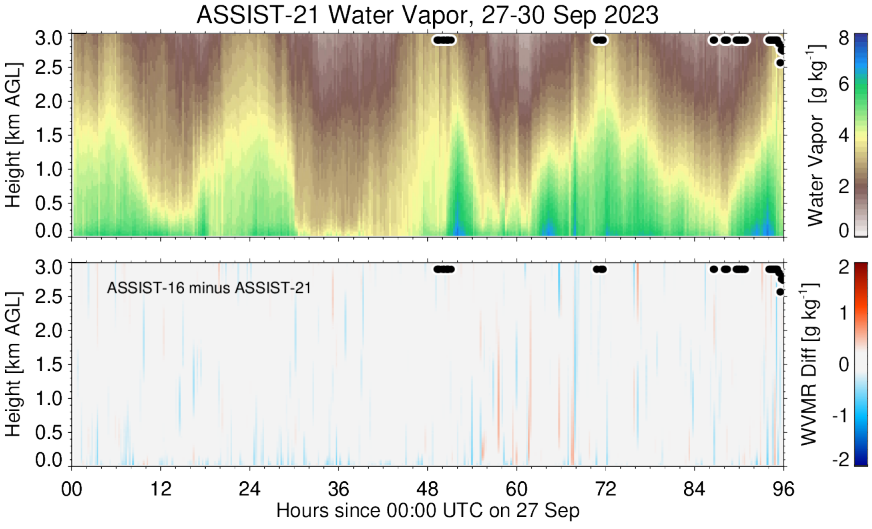

Figure 9: Same as Fig. 8, but for water vapor mixing ratio.

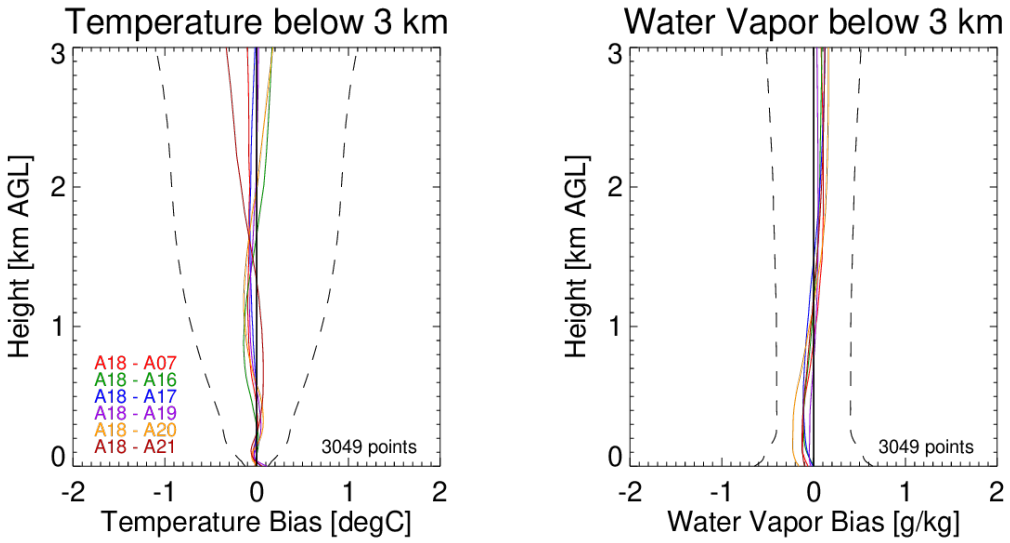

Figure 10: Mean differences in retrieved temperature (left) and water vapor (right) between other ASSISTs and the A18 unit during clear sky conditions. The dashed lines represent the 1-σ uncertainty in the *TROPoe* retrieval.

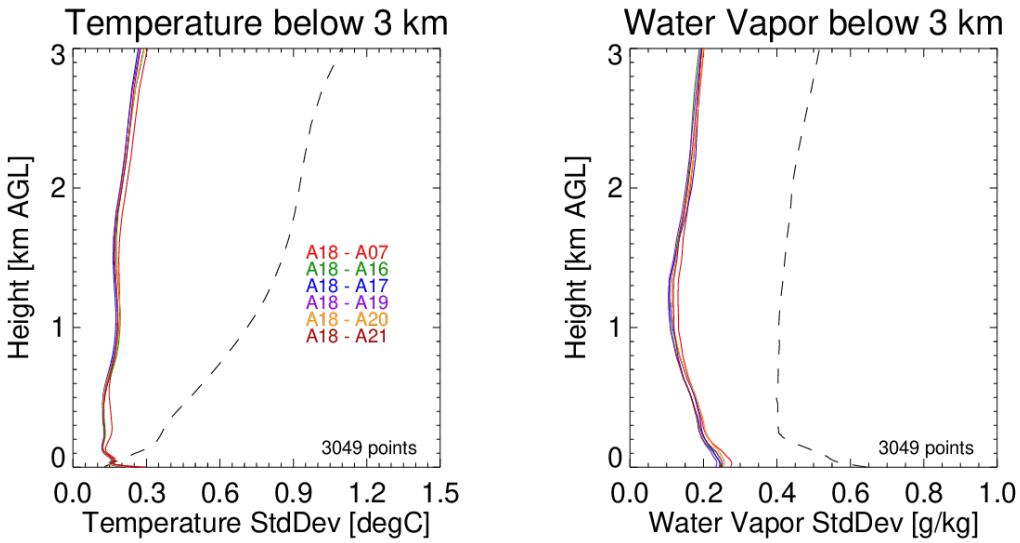

Figure 11: Standard deviation in the differences in retrieved temperature (left) and water vapor (right) between other ASSISTs and the A18 unit during clear sky conditions. The dashed lines represent the 1-σ uncertainty in the *TROPoe* retrieval.

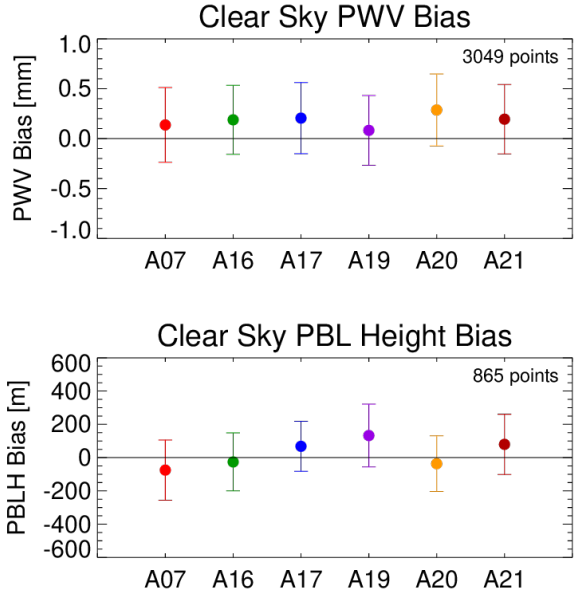

Figure 12: Differences in the PWV (top) and daytime PBLH (bottom) between the other ASSISTs and the A18 unit in clear sky conditions.

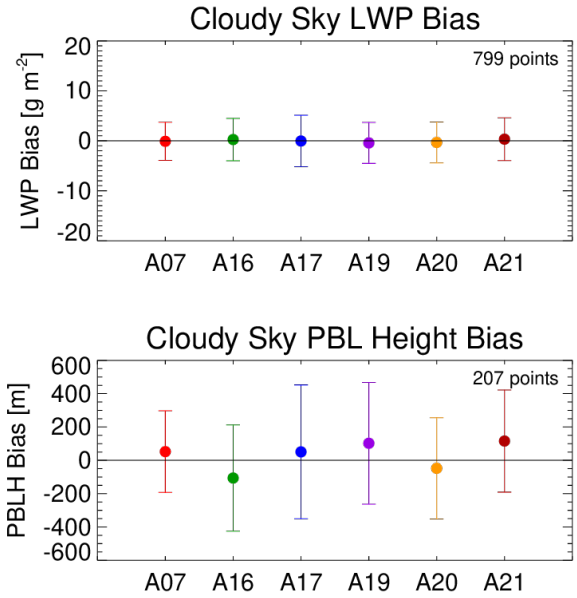

Figure 13: Differences in the retrieved LWP (top) and daytime PBLH (bottom) between the other ASSISTs and the A18 unit for cloudy conditions.

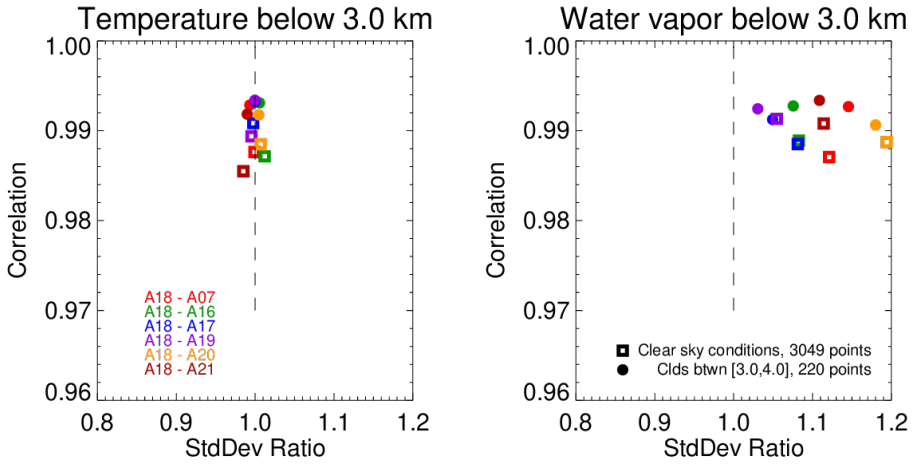

Figure 14: Modified Taylor plot showing the mean correlation and standard deviation ratio of the profiles of temperature (left) and water vapor (right) for heights below 3 km between the other ASSISTs and the A18 unit. Clear sky points are indicated by squares, and cloudy points are for conditions where the overhead cloud was between 3.0 and 4.0 km.